Tectonophysics 903 (2025) 230702

Contents lists available at ScienceDirect

Tectonophysics

journal homepage: www.elsevier.com/locate/tecto

Seismic reprocessing of BELCORP-DEKORP 1A reveals deep fault reflections of the Paleozoic Eifel Fold and Thrust Belt in Germany

D. Eickhoff [a,*], S. Back [b], K. Reicherter [c], J.R.R. Ritter [a]

[a] Karlsruhe Institute of Technology, Geophysical Institute, Germany
[b] RWTH Aachen, Geological Institute, Germany
[c] RWTH Aachen, Neotectonics and Natural Hazards, Germany

ARTICLE INFO

Keywords:
Seismic reflections
Tectonics
Eifel
Fold-thrust belt

ABSTRACT

The Paleozoic Eifel Fold and Thrust Belt is part of the northern Variscan Deformation Front. Due to erosion, parts of its uppermost layers have been removed, enabling direct seismic reflection imaging of its internal deformation pattern in the upper crust utilizing seismic reflection imaging techniques. Reprocessing of the BELCORP-DEKORP seismic reflection line 1A from 1987 reveals previously undocumented structural details when applying state-of-the-art tools such as an improved seismic velocity background model and Fresnel volume migration. Additionally, a detailed analysis of seismic polarities helps to characterize the impedance contrasts of the reflectors at depth. A marked reflector of approximately 80 km length is identified, originating in the Belgian Ardennes Mountains and terminating in the southeast in the Hocheifel Volcanic Field at a depth of c. 12 km. The reflector dips in average with about 8° towards the southeast and has a thickness of approximately 400 m. In many parts, this reflector is characterized by a negative impedance contrast, which can be interpreted as a fault gouge or breccia composed of crushed rock, possibly containing fluids. This large feature is interpreted as the basal detachment zone of a wedge-like structure. A restoration model of this wedge results in shortening of about 22 km. In addition to the main detachment reflector, numerous tectonic features like subsidiary fault strands, synclines, ramps and backthrusts have been imaged. Strong reflectors in the Hocheifel Volcanic Field are interpreted as solidified sills related to the Cenozoic magmatism.

1. Introduction

Over the past decades, the interpretation of the deformation front of the Variscan Orogen of central Europe has been a subject of recurrent debates, including among others a discussion of two end-member models that explain the tectonic signature and development of the Eifel Fold and Thrust Belt (Fig. 1). Based on field data (Fielitz, 1992), reflection seismic profiling (Meissner et al., 1981; Durst, 1985; Betz et al., 1988; DEKORP Research Group et al., 1991) and quantitative tectonic restoration (Von Winterfeld, 1994; Hollmann and Von Winterfeld, 1999; Oncken et al., 1999), several research groups interpreted the Eifel Fold and Thrust Belt as formed by thin-skinned tectonics above a major detachment with significant horizontal nappe displacement and shortening in the order of several tens of kilometres. In contrast, based on an extensive field, drilling and underground mining database, for example Wrede et al. (1993) and Wrede (2000) favoured a subsurface interpretation of the Variscan frontal zone as dominated by large-scale folding in the area of the Aachen Thrust near the city of Aachen, Germany (Fig. 1), accompanied by break-thrusts with minor horizontal displacement. Today, the prediction of the geological architecture of the fold-thrust front of the Variscan Orogen becomes increasingly important for applied studies focusing on geothermal subsurface exploration, as well as the possible subsurface construction of a large gravitational wave detector, the Einstein Telescope (e.g., Bader et al., 2022).

Essential data interpreted for analysis of the Variscan Orogen are long-range deep-reaching seismic-reflection lines measured across Germany and bordering countries in the 1980s and 1990s within the European Continental Reflection Seismic Programme (DEKORP in Germany and BELCORP in Belgium; Meissner et al., 1981; Meissner and Bortfeld, 1990; Meissner, 1991). Of these, BELCORP-DEKORP line 1A (Fig. 1) covers the western part of the Variscan Rhenish Massif starting in Belgium within the Stavelot-Venn Massif (SVM) close to the Belgian-

* Corresponding author.
E-mail addresses: dario.eickhoff@kit.edu (D. Eickhoff), back@geol.rwth-aachen.de (S. Back), k.reicherter@nug.rwth-aachen.de (K. Reicherter), joachim.ritter@kit.edu (J.R.R. Ritter).

https://doi.org/10.1016/j.tecto.2025.230702
Received 21 November 2024; Received in revised form 28 February 2025; Accepted 5 March 2025
Available online 7 March 2025

Dutch border. The seismic line trends in NW-SE direction, traversing the Eifel Mountains, and terminates in the near vicinity of the town of Adenau in the Cenozoic Hocheifel Volcanic Field (Fig. 2; HEVF). The initial processing and interpretation of line BELCORP-DEKORP 1 was limited to time migration and revealed both shallow and deep-reaching faults related to the deformation of the northern Variscan front (e.g., Meissner et al., 1981; Hance et al., 1999; Oncken et al., 1999). The upper crust was found to be more transparent, while the lower crust was reflective, which is consistent with the characteristics of Variscan terranes (e.g., Meissner, 1991). Today, all DEKORP recordings are stored at the DEKORP Data Archive at GFZ Potsdam, Germany (Stiller et al., 2020), and can be used for reprocessing and reinterpretation purposes (see for BELCORP-DEKORP line 1A e.g. Arndt et al., 2023), allowing users to apply the most recent processing techniques to this unique dataset.

In 2004, the 2544 m (measured depth along the borehole) deep well RWTH-1 was drilled in the urban centre of Aachen approximately 15 km east of BELCORP-DEKORP line 1A (Figs. 1, 2). The borehole is located on the campus of RWTH Aachen University providing a unique geological insight into deeper subsurface geology of the Aachen area (e.g., Trautwein-Bruns et al., 2010; Trautwein-Bruns et al., 2011). This study presents a reinterpretation of reprocessed DEKORP seismic-reflection data integrated with this relatively recent deep-borehole information and modern geological field observations. The data and work presented provide new constraints for interpreting the Paleozoic subsurface beneath the Eifel mountains, ultimately enabling a re-evaluation of existing surface-subsurface models of the northern Variscan Eifel Fold and Thrust Belt.

2. Geological framework

The Rhenish Massif is part of the Central European Variscan Orogen (Fig. 1). The Eifel Fold and Thrust belt represents the northwestern front of the Rhenish Massif (Figs. 1, 2). In the west, the Paleozoic of the Rhenish Massif is directly connected with the Ardennes, which are presently forming a prominent peneplain, the Rhenish shield. The primary geological structures of the Eifel Fold and Thrust belt are the WSW-ENE oriented Aachen Thrust and Stavelot-Venn anticline in the NW, and the Mid-Devonian limestone synclines in the SE (Fig. 2). The Stavelot-Venn Anticline is composed of the oldest rocks of the Rhenish Massif, namely the orogenic core consisting of rocks of Cambrian and Ordovician ages is flanked both in the NW and SE by a kilometre-thick Devonian sedimentary succession, which in the east is overlain by Carboniferous clastics and carbonates (Fig. 2). The stacked Paleozoic succession of the Rhenish Massif is repeatedly exposed in the Variscan fold-and-thrust belt due to the predominance of NW-verging folds and primarily SW-dipping thrusts (Fig. 2). Between 336 Ma and 300 Ma, this part of the Rhenish Massif underwent complex deformation and low-grade metamorphism. Previous balancing studies have estimated the maximum overall shortening to be approximately 45 % (Hollmann and Von Winterfeld, 1999).

In the E, remnants of Mesozoic sequences are exposed in the 'Mechernich Triassic Triangle' area, including sandstones, siltstones, shales and limestones belonging to the Triassic Buntsandstein (Bunter), Muschelkalk, and Keuper formations (Fig. 2). In the NW, deformed Paleozoic rocks (Fig. 2) are covered by Cretaceous Units and the Cenozoic sediments of the Lower Rhine Embayment (Fig. 1), and displaced by

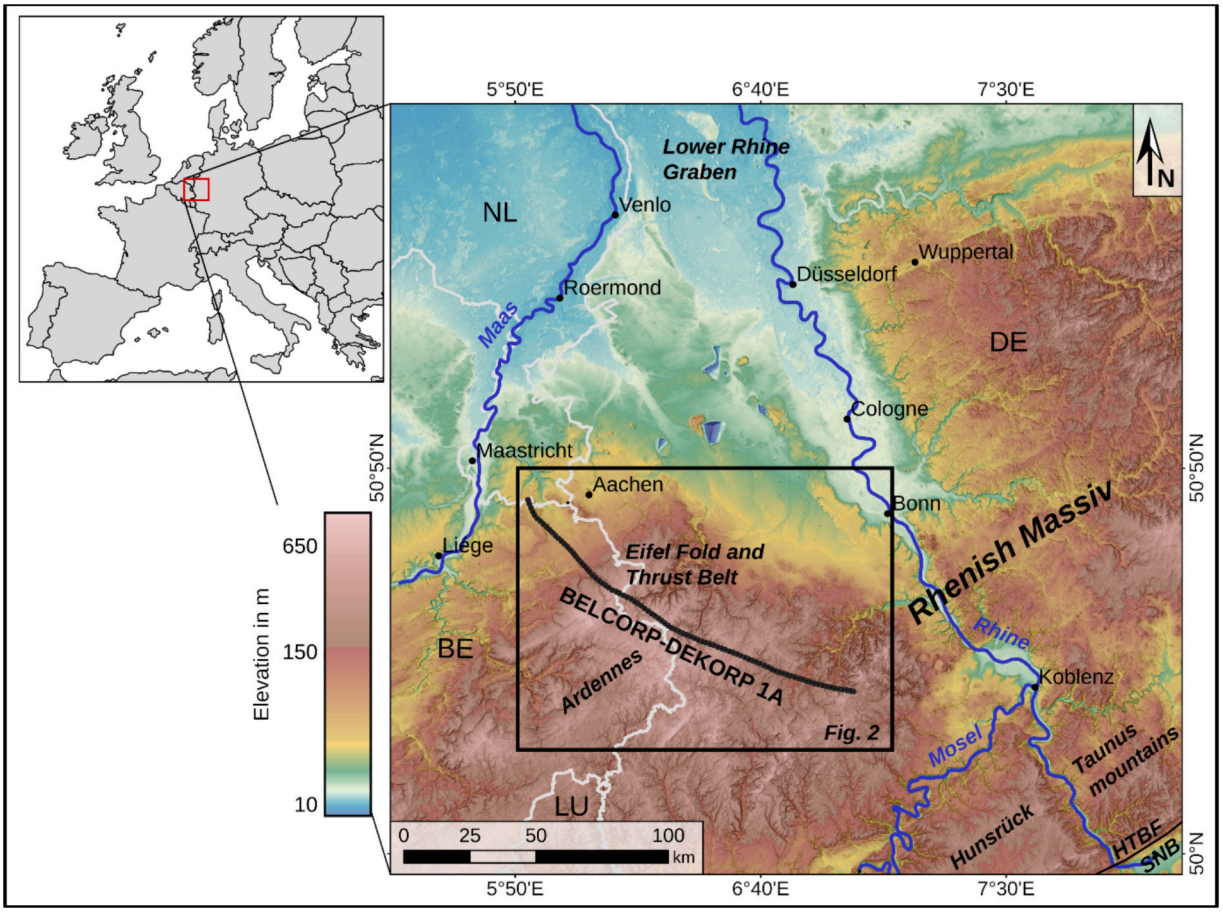

Fig. 1. Topographic map of the study area. The Eifel Fold and Thrust belt is situated on the western Rhenish Massif in the border region of Belgium (BE), Germany (DE), Luxembourg (LU) and the Netherlands (NL). SNB: NE end of the Saar-Nahe Basin. HTBF: Hunsrück Taunus Boundary Fault. Inset map shows study area in central Europe.

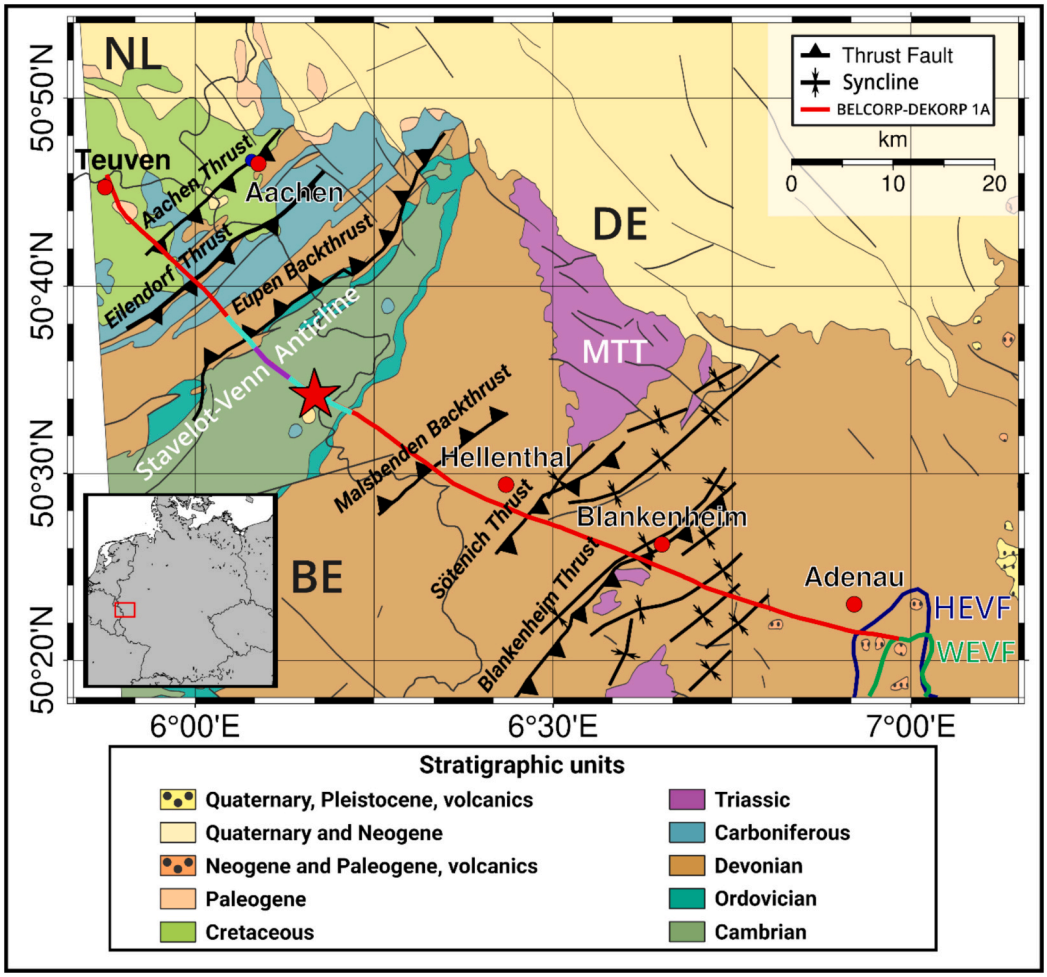

Fig. 2. Geology map of the study area with major faults (for larger context see Fig. 1) and BELCORP-DEKORP line 1A. The position of shot 577 (Fig. 3) is marked with a red star, the shot geophones are turquoise and the seismic traces in Fig. 3 shown were recorded in the purple line section. MTT: Mechernich Triassic-Triangle. HEVF (dark blue): Hocheifel Volcanic Field. WEVF (green): West Eifel Volcanic Field. Data from Voges et al. (2006). (For interpretation of the references to colour in this figure legend, the reader is referred to the web version of this article.)

Cenozoic NW-SE trending normal faults of the Lower Rhine Graben (Reicherter et al., 2008). In the Eifel, two volcanic intervals occurred in the Cenozoic HEVF at c. 44–39 Ma and 37–35 Ma (Fekiacova et al., 2007). Later the two Quaternary West and East Eifel Volcanic Fields (WEVF, EEVF) became active around 700 kyr ago (Schmincke, 2007). This activity has been related to a mantle plume (Ritter et al., 2001). The Laacher See eruption (EEVF) at c. 13,000 cal yr BP (Reinig et al., 2021), and about 70 other eruption centres within in the WEVF since the last 70 kyr represent the youngest active volcanoes in Germany. To the S, the Rhenish Massif is separated from the Late Paleozoic of the Saar-Nahe Basin by the Hunsrück Taunus Boundary Fault that runs along the southern edge of the Hunsrück and Taunus mountains (Henk, 1993; Fig. 1).

3. Data & methods

3.1. Data acquisition

The 2-D BELCORP-DEKORP seismic-reflection line 1A (referred to hereafter as “line 1A”) is 93 km in length and starts in the N, in the vicinity of the village of Teuven, Belgium (Fig. 2). Line 1A continues from Belgium into the German Eifel mountains south of Aachen and proceeds in a southeasterly direction towards the town of Adenau. The line intersects several geological structures: in the NW, line 1A is perpendicular to the northern Variscan front and the Stavelot-Venn Massif including the Eifel Fold and Thrust belt (Fig. 2); in the SE line 1A crosses the Eifel North-South Zone and runs perpendicular to several fault zones that bound the Eifel limestone synclines to the HEVF (DEKORP Research Group et al., 1991, Fig. 2).

The seismic-reflection data were recorded using a vibroseis source and a maximum of 400 geophones per source point (Stiller et al., 2020). For each source point, the geophones were oriented in an asymmetric split-spread configuration, with one side of the spread occupied by 300 geophones and the other side by 100 geophones. The spacing of the geophones, at 40 m, results in a spread with a total length of 12 km on one side and 4 km on the other side. The vibroseis source excitation was performed with the use of five trucks and fivefold vertical stacking per source point as a linear sweep with a duration of 20 s and a frequency band of 12–48 Hz. Following the 20 s sweep, an additional 16 s of listening time was recorded in order to capture incoming signals from as deep as the lower lithosphere. The short offsets ensured a nearly vertical beam path for large depths exceeding 30 km below the area of the respective measurement point. A total of 1891 vibration points were utilized with a spacing of 40 m, resulting in an up to 200-fold coverage (Stiller et al., 2020).

3.2. Reflection processing

Before migration of the seismic-reflection data, we performed time-domain signal processing of the data set. Details of the data processing

are described in Eickhoff et al. (2024). Reflections were amplified and undesired parts of the wavefield removed or attenuated (Fig. 3). The processing steps used were bandpass filtering using the corner frequencies of the vibroseis sweep, to make sure that the correlation was done correctly. A trace normalization was performed to equalize the amplitudes of the individual seismic traces with each other. In addition, amplitudes were time-scaled to enhance later arriving reflected onsets. Finally, the amplitudes of wavefields, that would interfere with the migration operation were suppressed, such as the first arrivals and air-blast noise. Additionally, deconvolution and denoising operations were applied to further increase the signal-to-noise ratio. Deconvolution operations were used to remove noise within the frequency band of the vibroseis sweep (i.e., 12–48 Hz), while denoising removed outliers in the time-frequency domain.

A 2-D first-arrival travel time tomography was performed along line 1A to determine a P-wave velocity (*vp*) model extending up to c. 750 m in depth for the depth migration. A crustal velocity model is used for the migration below this depth. The crustal velocity model was derived from a long-range seismic refraction experiment (Mechie et al., 1983). The two *vp* models were smoothed to remove strong discontinuities, particularly at the transition from the shallow tomography velocity model to the deeper crustal velocity model. The migration of the time-domain dataset transformed the recorded reflections into reflectors in depth. The migration method applied was a Fresnel Volume Migration (FVM), which is a modification of the standard Kirchhoff migration (Buske et al., 2009). In this way images of the Kirchhoff migration can be improved by limiting the migration operator to the actual Fresnel volume of the wavefield in depth. This operation is achieved by utilizing the emergent angle at the receiver (Buske et al., 2009). Limiting the migration operator helps to improve the image quality, because the smearing along the two-way travel time isochrons is constrained to the actual reflection point at depth, whereas the whole isochron would be used in standard unmodified Kirchhoff migration (Bleistein and Gray, 2001). The migration images, generated with the combined seismic velocity models, display structures at high resolution throughout the upper crustal region beneath the surface profile and minimize artifacts in shallow depths. In the following sections, the high-resolution depth image produced will serve as the basis for structural and stratigraphic interpretation.

The amplitudes of the reflected signals are normalized as stacked energy (NME, 0–1) to display the strength of the reflections. In addition, the polarities of the reflected signals are analysed to determine the type of impedance contrast (positive / negative) of the reflectors (see supplement).

The spatial resolution of the imaged structures, particularly the vertical uncertainties, is largely dependent on the seismic velocity model applied for migration. Deep reflections are less well constrained, because there, seismic waves must propagate a longer distance through the unknown seismic velocity structure. We estimate the uncertainty of the vertical resolution of our subsurface images to be in the order of ±400 m in the upper crust (depths of up to 15 km), and with greater depths resulting in increased uncertainty. Due to the configuration of the near-vertical seismic experiment the lateral resolution should be superior to the vertical one. We estimate lateral uncertainties to be ±200 m. Furthermore, the proportionally increased attenuation of higher frequencies also has a negative effect on the accuracy of the vertical resolution. A third limiting factor for the vertical resolution is the dominant frequency of 20 Hz used for the migration operation, because the estimation of the reflector thickness is bound to the dominant frequency of the FVM. We estimate that this uncertainty is approximately one wavelength, or ± 200 m. The measured dip of the structures depends on the vertical and lateral resolution of the migration image. The resulting estimated uncertainty in dip ranges within ±2°.

4. Results

4.1. Section overview

Fig. 4 provides an overview of the FVM seismic image along BELCORP-DEKORP line 1A between Teuven (Belgium) in the northwest and Adenau (Germany) in the southeast (Fig. 2). The FVM display in NME emphasizes reflections mostly related to tectonic structures instead of stratigraphic features, similar but complementary to reflection attributes such as variance or coherency. The main reflection feature visible is a continuous, SE-dipping reflector with a minimum length of 80 km. The main reflection can be further subdivided into five main segments, designated A, B, C, D and G, from the northwest to the southeast (Figs. 4 and 5). Adjacent reflectors and segments are further subdivided into individual subsegments, which are indicated by numbers (Figs. 4b and 5). The main reflector is composed of first-order reflectors and subsegments A1, A2, B1, B2, B3, C1, C2, D1, and G. The physical parameters of these subsegments are described in the following section, along with those of some other prominent subsegments. Further details are provided in the supplement.

4.2. Classification of the reflectors

In order to get first overview of the reflectors and their possible origins, we classify them into the three following classes: tectonic (faults, detachment), stratigraphic (synclines) and magmatic (e.g., intrusions, sills). Tectonic reflectors are preliminary assigned to structures close to known faults and expected dips. Especially near to sedimentary stratigraphic reflectors are expected. In the Hocheifel Volcanic Field (HEVF), at the eastern end of the line, magmatic intrusions with strong impedance contrasts are known (Eickhoff et al., 2024). Furthermore, structures below the detachment are not classified, due to the ambiguous geological context there. For the purpose of classification, we use geological maps (e.g., Nordrhein-Westfalen Geologisches Landesamt,

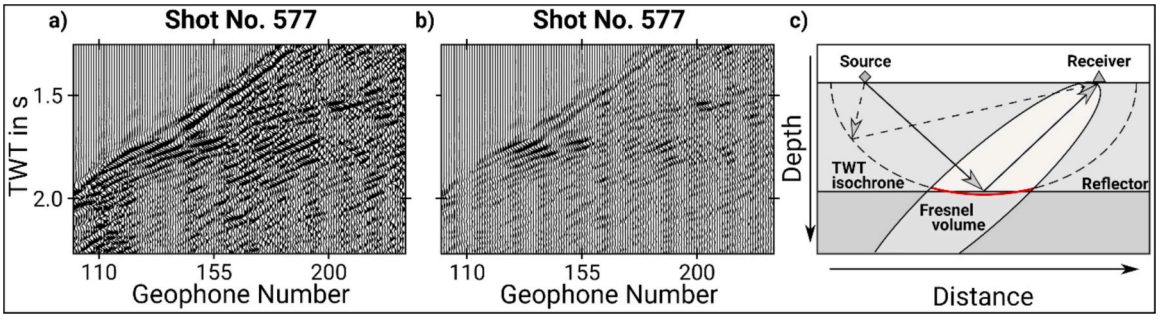

Fig. 3. Amplification of reflections and attenuation of the remaining wavefields (e.g., ground roll) to prepare the dataset before migration. a) recordings from shot 577 (for location see red star in Fig. 2) before pre-processing, b) after pre-processing, c) sketch of Fresnel volume migration modified from Buske et al. (2009). The red line corresponds to the top of the migrated reflector based on wave path and frequency of the signal. (For interpretation of the references to colour in this figure legend, the reader is referred to the web version of this article.)

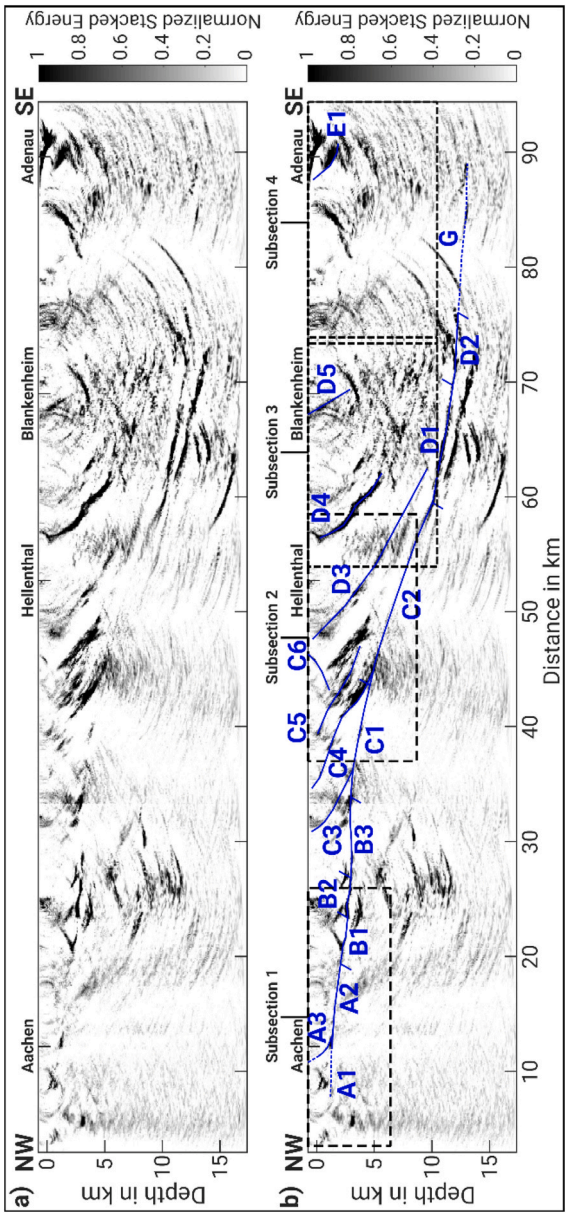

Fig. 4. a) Uninterpreted Fresnel volume migration (FVM) section along BELCORP-DEKORP line 1A without vertical exaggeration; b) interpreted FVM section with labelled main reflection segments (letters) and subsegments. The subsections 1–4 (dashed frames) are presented in Fig. 5 in an enlarged view; for detailed descriptions see the supplement (Figs. S2–S5). Reflection amplitudes are displayed as normalized stacked energy (NME).

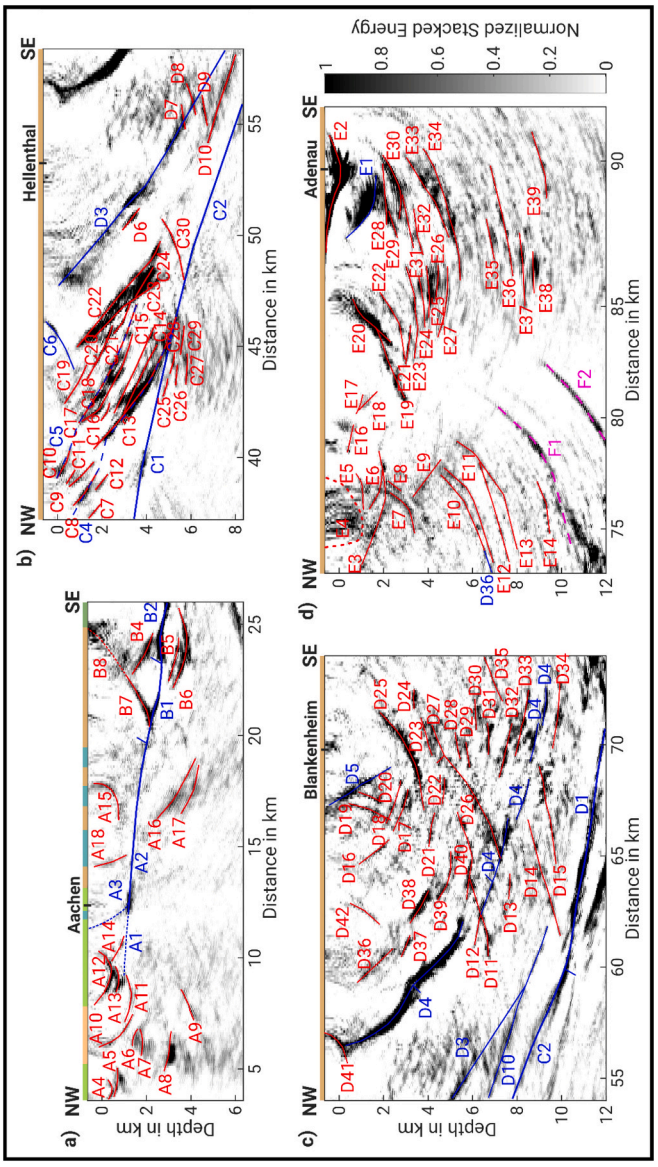

Fig. 5. Detailed view of FVM subsections 1–4 (a-d); reflectors are labelled according to their occurrence from NW to SE in five segments A to E with a further subdivision in subsegments (numbers). Marked in blue are large scale reflectors (also shown in Fig. 4), small scale reflectors are marked in red. A detailed description of all marked reflectors and their properties is provided in the supplement. Colour coding at the surface corresponds to the stratigraphic units (see Fig. 2). (For interpretation of the references to colour in this figure legend, the reader is referred to the web version of this article.)

1992) and previous interpretations (e.g., DEKORP Research Group et al., 1991; Dahm et al., 2020) together with the physical parameters outlined in Section 4.3.

4.3. Details of the main reflectors

Reflector A1 is located at the NW end of BELCORP-DEKORP line 1A at c. line kilometre 7 in a depth of c. 1.1 km (Figs. 4b and 5a). A1 extends laterally for c. 3.5 km and it dips slightly towards the SE with 2°. A signal polarity could not be recovered for A1. In the following, if signal polarities could not be recovered, they are omitted. Negative polarities indicate a low impedance contrast (hence low density material or low seismic velocity), and positive polarities indicate denser material or high seismic velocity in comparison to the surrounding rock. A2 starts at the eastern end of A1 and extends over 8.3 km in a depth of 1–2.2 km with a dip of c. 5° towards SE. Its strength (NME) is 0.3 and its thickness is c. 400 m (Fig. 5a). Reflector A3 is an upward side branch of the main reflector in a depth of 1 km. It extends almost to the surface south of Aachen. Even though the uppermost 250 m cannot be well resolved, a continuation of the reflector to the surface is likely (Figs. 2, 5, S2). The length of A3 is c. 1.7 km and its dip varies from 60° SE to 23° SE with a steeper dip angle at the top side of the reflector.

Reflector B1 is located at the eastern end of A2 with a length of 2.4 km in a depth of 2.2–2.6 km (Figs. 4b and 5a). B1 dips with 5° towards SE and it is c. 400 m thick. The sign of the related reflection signal is negative (Fig. S7b) and its strength (NME) is 0.4. Reflector B2 extends from line kilometres 22.4–26.8 in depths of 2.6–3 km (Figs. 4, 5a, S2). Its dip varies between 5° to NW and 2° to SE, which means that this reflector most likely lies almost horizontally given the dip uncertainty. The strength (NME) of B2 is 1, thus it has the maximum impedance

contrast, and the polarity of the reflection signal is mostly negative throughout the NW-SE extent of the reflector. B2 is c. 600 m thick (Fig. 5a). B3 is located beneath the area of the Stavelot-Venn Massif (Fig. 2) and it laterally extends 6.8 km towards the SE in a depth of c. 2.9 km. Reflector B3 is almost horizontal and it is c. 500 m thick. The strength (NME) of the reflector is 0.4 and its reflected signal polarity changes from negative to positive with increasing horizontal distance, which implies a lateral change in density/seismic velocity.

Reflector segment C is located between line kilometres 33.6–60 and it consists of two long eastward dipping reflectors C1 and C2. C1 is located between kilometres 33.6 and 43 (Fig. 5b) with a length of c. 9.6 km in varying depths of 2.9–4.7 km. It is 400 m thick and dips with 10° to E. The reflection polarity is mostly positive and the strength (NME) about 0.2. From the southern end of C1, reflector subsegment C2 extends 17.3 km laterally towards the SE in depths of 4.7–10 km (Fig. 5b). C2 is 400 m thick and has a dip of 18° towards SE. Its reflection polarity is mostly negative (Fig. S7e) and the reflection strength (NME) of C2 is 0.3.

Further SE the main reflector continues as the deep segment D below the area around the town of Blankenheim (Figs. 4, 5c): subsegment D1 is located between line kilometres 59.5 and 69.5 in depths of 10–11.8 km with a length of 10.2 km and a thickness of up to 600 m (Figs. 5c, S4). D1 dips with 10° to SE and its polarity sign is mostly negative throughout the extension of the reflector. The reflection strength (NME) of D1 is 0.6. From the SE end of subsegment D1, reflector D2 extends 6 km laterally further towards SE in depths of 11.8–12.6 km (Fig. 4). It is 400 m thick and dips with 4° SE. The reflection sign of D2 is positive and negative (Fig. S7g) and its strength (NME) is 0.5.

Reflector G (Fig. 4b) is the lowest part of the main reflector which seems to reach the HEVF near Adenau. It has similar dips as subsegments D1 and D2. G extends from profile kilometres 75.5 to 89 in depths of 12.4–13.2 km. Reflector G is 400 m thick and 13.5 km long. The reflector dips with 3° E and has a strength (NME) of 0.3. The reflection polarities at G are positive. The low reflection strengths may be related with the stronger reflectors (see subsection 4 in Fig. 5d) at shallower depths which dampen the descending seismic wavefield before it reaches reflector G.

Besides the main reflector, additional prominent features above the main reflection feature are identified, namely C3-C6, D3-D5 and E1.

Reflector C3 is located between profile kilometres 31 and 36 in a height of −0.2 km to a depth of 2.9 km above reflector B3 (Fig. 4b). It is c. 300 m thick, and its dip increases towards the surface from 26° SE to 53° SE. Its reflection strength is 0.3. To the SE reflector C4 extends between profile kilometres 34.8 and 44.9 in a depth of −0.2 km to 4.9 km with a thickness of c. 400 m and a varying dip of 20° SE to 42° SE (Fig. 4b). The highest dip of C4 occurs below reflector C5 and its reflection strength is 0.5 with a positive sign.

Between profile kilometres 39.9 and 47.2, reflector C5 is located in a height of −0.1 km to a depth of 4 km (Fig. 4b). It is c. 500 m thick, and its dip increases upwards from 20° SE to 33° SE. The sign of the reflection polarity is positive with a strength of 0.5. Dipping in opposite direction (29 to 41° NW) reflector C6 stretches from profile kilometres 45.1–46.1 in a height of −0.5 km to a depth of 0.4 km. It is c. 300 m thick, and it has a low reflection strength of 0.1 (Fig. 5b).

Above D1 and D2, there are reflectors D3, D4, and D5. Subsegment D3 is located between profile kilometres 47.5 and 58.0 in depths of 0–8.3 km (Fig. 5b). It is c. 500 m thick, and it dips 27° to 41° E. The reflection polarity is positive, and its strength is about 0.4. Further SE, reflector D4 is in depths of 0.3–5.6 km with a lateral extension of 8 km and a thickness of c. 600 m (Fig. 5c). D4 dips with 16–73° towards the E with an increasing dip angle towards the surface. The polarity of the reflection sign of D4 varies along the extent of the reflector and its strength is about 0.7. To the SE, reflector D5 is located between profile kilometres 67.4 and 69.0 in a height of 0.2 km to a depth of 2.3 km. D5 is c. 400 m thick and has a lateral extension of 1.6 km and dips 58° E. It has a strength of about 0.6.

At the SE end of line 1A, reflector E1 is located below the HEVF near Adenau town in shallow depths of 0.3–1.6 km where it extends laterally over 3 km (Fig. 5d). Reflector E1 is c. 400 m thick and it dips 2–47° SE with increasing dip towards the surface. The reflection strength of E1 is 0.4. Further reflectors are described in the supplement.

5. Geological interpretation

The reprocessed BELCORP-DEKORP line 1A is dominated by a SE dipping detachment reflector (Meissner et al., 1981; Durst, 1985; Bois et al., 1986; DEKORP Research Group et al., 1991; Le Gall, 1992; Von Winterfeld and Walter, 1993; Von Winterfeld, 1994; Dahm et al., 2020) that dips gently to the S with <3° (Fig. 4). Towards the SE two broad ramp zones are developed (A3 and C5, D3, D4) with steeper dips. The northern ramp (reflectors A1 and A2) dips around 10° between line kilometres 10 and 20, the southern ramp (reflectors C1 and C2) has dips of up to 19° between line kilometres 40 and 60 (Fig. 4).

Many of the prominent main reflectors reach down to the detachment reflector (Fig. 4); the correlation of these reflectors at their upper tip to surface structures from geological reports and maps (Von Winterfeld and Walter, 1993; Von Winterfeld, 1994; Nordrhein-Westfalen Geologisches Landesamt, 1992; Ribbert, 2010) leads to following subsurface-surface interpretation (Fig. 6): reflector A3 (Fig. 4) corresponds to the Aachen Thrust (Von Winterfeld, 1994; Oncken et al., 1999; Fig. 6); reflectors B7 and B8 (Fig. 4) to the Eupen Backthrust (Nordrhein-Westfalen Geologisches Landesamt, 1992; Fig. 6). Reflector C3 (Fig. 4) corresponds to the Venn Thrust (Von Winterfeld, 1994; Fig. 6). Reflector C4 (Fig. 4) potentially corresponds to an intra-Cambrian thrust in the Western Hürtgen Forest (Fig. 6; Von Winterfeld, 1994; Ribbert, 2010). Reflector C5 (Figs. 4, 5a) can be correlated to the Eifel Nappe Base Thrust of Von Winterfeld (1994); reflector C6 (Fig. 4) to the Malsbenden Backthrust (e.g., Von Winterfeld, 1994; Ribbert, 2010; Fig. 6). Reflector D3 (Fig. 4) likely corresponds to the Schleiden Thrust of Von Winterfeld (1994); this structure is probably blind (Figs. 4 and 6), i.e., its upper tip is not clearly documented at surface (Ribbert, 2010). Reflector D4 (Fig. 4) corresponds to the Sötenich Central Thrust (Figs. 5c and 6; Von Winterfeld, 1994; Ribbert, 2010); reflector D5 (Figs. 4, 6) to the Blankenheim Thrust (Fig. 6; Ribbert, 2010). In the very SE of line 1A, there are several reflectors (E1, E2 and the series E28-E39; Fig. 5d) which likely image shallow intrusions of the HEVF near Adenau (Fig. 6).

In comparison to existing studies (e.g., Meissner et al., 1981; Durst, 1985; Bois et al., 1986; DEKORP Research Group et al., 1991; Le Gall, 1992; Von Winterfeld and Walter, 1993; Von Winterfeld, 1994; Dahm et al., 2020; Arndt et al., 2023), several of the previously suspected structural elements are now clearly imaged on reprocessed BELCORP-DEKORP line 1A; allowing in many places an updated tectonic subsurface interpretation. Among the key differences in comparison to the previous data presentations and (sub)section interpretations are:

i) the observation of an abundance and frequency of suspected overburden faults above the steepest parts of the detachment reflector (Fig. 6);
ii) the observation of a kilometre-scale backthrust touchdown onto the detachment reflector (B2 – Eupen Fault; Fig. 6);
iii) the detachment reflector in the frontal thrust belt below the city of Aachen in c. 2000 m depth, as opposed to its previous prediction at c. 4 km depth (e.g., Oncken et al., 1999);
iv) a lower root of the Malsbenden Backthrust (C6) in c. 2000 m depth probably connecting to the Eifel Nappe Base Thrust; and the Malsbenden Backthrust likely truncating the inferred Schleiden blind thrust (C5; Figs. 5 and 6) in the shallow subsurface;
v) a multitude of previously undiscovered reflectors of varying strength between line kilometres 60 and 80 (Figs. 4, 5 and 6);
vi) very strong seismic reflectors around line kilometre 90 in the upper 1.5–2 km depth underneath the region of Adenau and underneath (to c. 10 km depth) further SE-upwards dipping reflectors which are most probably related to magmatic intrusions

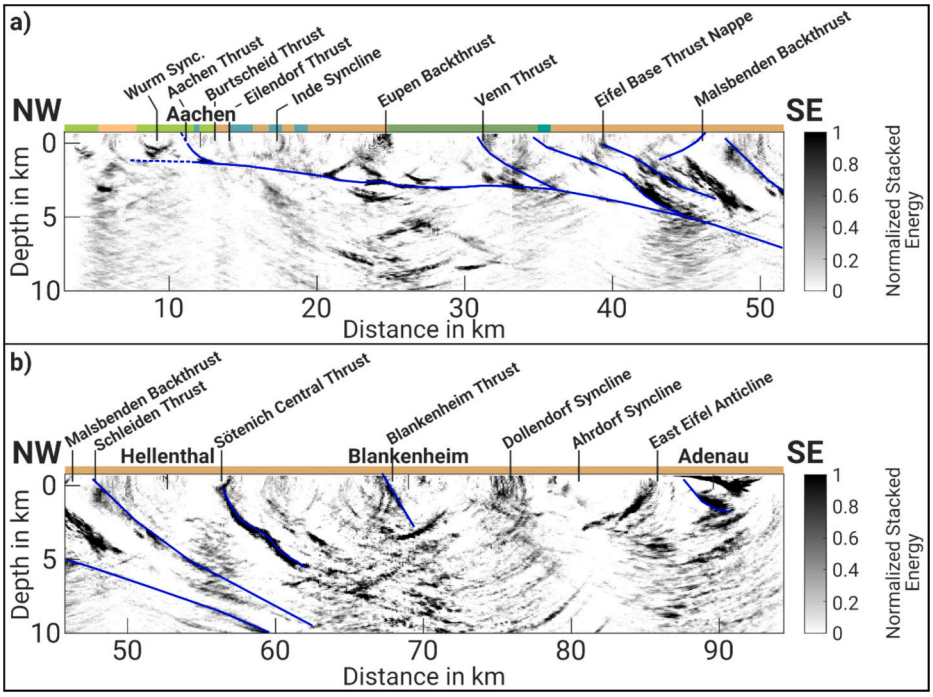

Fig. 6. a) Northwestern part of the FVM section along BELCORP-DEKORP line 1A with near surface parts of main reflections correlated with known surface structures; b) southeastern part of the FVM section along BELCORP-DEKORP line 1A. Both profiles overlap near the surface location of the Malsbenden Backthrust. Colour coding at the surface corresponds to stratigraphic units (see Fig. 2); no vertical exaggeration is applied.

related to the HEVF. This stack of intrusions is imaged for the first time this clearly.

Besides regional geological interpretation, the new, detailed subsurface image of the regional detachment of the Eifel Fold and Thrust belt by the reprocessed BELCORP-DEKORP line 1A provides a valuable constraint for tectonic balancing. For example, thrust-wedge balancing sensu Yang et al. (2022) can be used to restore a section to the initial geometry of a trapezoid. This simple approach explores the effects of changing the dip of the wedge top (regional slope) and basal slope (Fig. 7) on shortening estimates, taking in this Eifel case study advantage of the very clear image of the wedge base (detachment). Key variable is

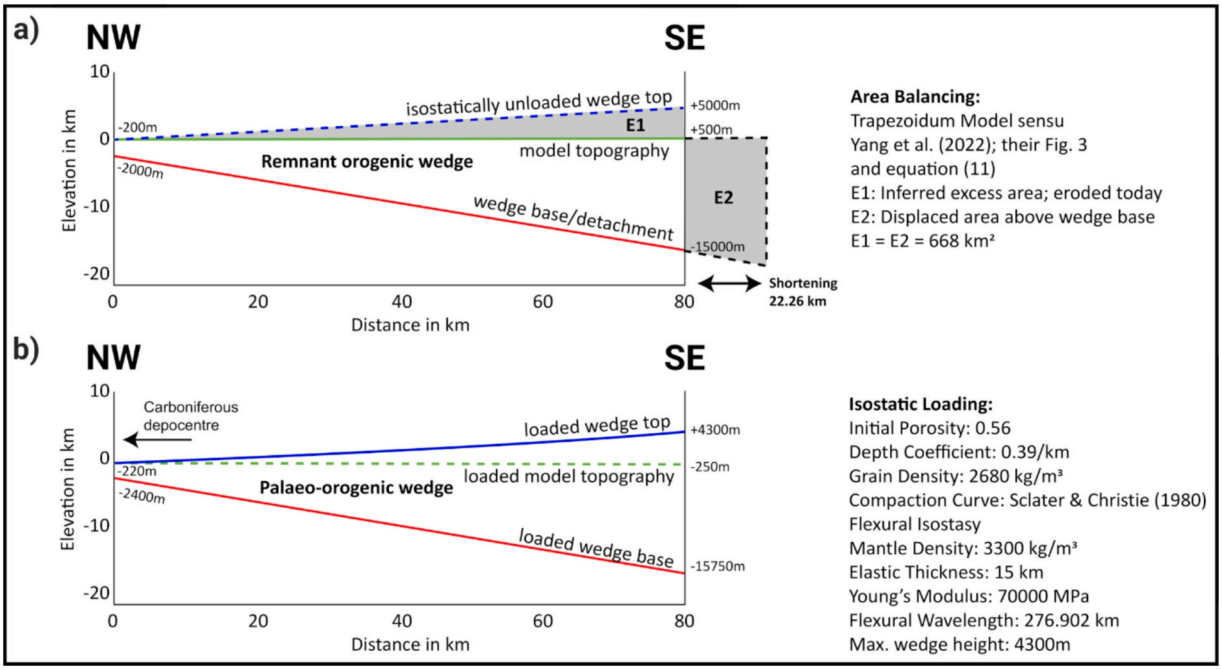

Fig. 7. a) Area balancing (trapezoidum model sensu Yang et al., 2022) with inferred Paleozoic orogenic wedge of up to 5 km height. Burial of present-day land surface (model topography) in line with coal-rank data and metamorphic isograde analysis of Oncken et al. (1999). Excess area 1 (E1) equals displaced area above wedge base (E2). Calculated wedge shortening is >22 km. b) Simplified Variscan orogenic wedge geometry along BELCORP-DEKORP line 1A, restored from a) by isostatic loading and compaction.

the Paleozoic paleo-topography of the Eifel mountains. The topography of today is on average between 200 m above sea level in the NW and 500 m above sea level in the SE, constituting an erosional remnant morphology influenced by many processes unrelated to Variscan mountain building. These uplift processes include relatively recent, e.g., Cenozoic, uplift by magmatic processes (e.g. Garcia-Castellanos et al., 2000; Meyer and Stets, 2007; Kreemer et al., 2020; Silverii et al., 2023), potentially in combination with post-Pleistocene isostasic adjustment or large-scale lithospheric folding (Demoulin and Hallot, 2009). The height of the Paleozoic top of the Eifel Fold and Thrust Belt can be reconstructed by coal-rank vitrinite-reflectance data of outcrop samples between Aachen and the southern Hunsrück area (location Fig. 1; data from Oncken et al., 1999). The coal rank in the study area is generally low (meta-anthracite stage), and associated peak temperatures are mostly between 150 °C and 250 °C (Oncken et al., 1999). These temperatures suggest burial of the fossil Eifel Fold and Thrust Belt of less than 10 km (assuming a default geothermal gradient of 30 °C/km). Fig. 7a shows a simplified area-balancing example restoring a wedge of 200 m (NW) to 4.5 km (SE) of compacted rock material on top of the present-day Eifel Mountain topography; producing an excess area of c. 670 km^2 (after Yang et al., 2022) which equals wedge shortening by about 22 km when restoring the paleo-topography to sea level. Fig. 7b shows the result of exactly this scenario when using the estimated thickness above the current topography as isostatic load. Such loading would have reduced peak elevation from 5000 m to c. 4300 m in the Eifel hinterland, depressing the detachment level in the NW from 2000 m to 2400 m, and in the SE from 15,000 m to 15,750 m. The loaded wedge top shown is a fast-track balancing estimate of the average topography of the Eifel mountains at the orogenic peak before >300 Ma of rather constant erosion.

6. Discussion

Seismic reprocessing of the BELCORP-DEKORP line 1A dataset results in an improved reflection imaging in comparison to the original processing approach (e.g., DEKORP Research Group et al., 1991). In comparison to previous reprocessing, e.g. by Dahm et al. (2020) or Arndt et al. (2023), we apply a new seismic velocity model (Eickhoff et al., 2024) and use FVM, which resolves key reflections very clear and images new reflectors in the upper 10 km of the subsurface. Reprocessing enabled the interpretation of subsurface reflections in a tectonic, stratigraphic or magmatic context, with precise information about the length, strength and dip angle of the individual reflectors. This information was used for schematic geometric balancing of the Eifel Fold and Thrust Belt (Fig. 7).

Seismic reflectors located between line kilometres 85 and 92 (E1, E2 and E28-E39; Figs. 4, 5d) are located below the HEVF and are interpreted as of magmatic origin (Table 1). Their partly strong impedance contrasts and their mostly subparallel structure indicate these features have a sill-like intrusive character. The subparallel reflectors E28-E39 may represent a series of solidified sills, as observed in other regions (e.g., near the Faroe Islands, White et al., 2008) and beneath the WEVF in Germany (Eickhoff et al., 2024). The HEFV intrusion zone (Fig. 5d), which is also identified as a local magnetic high and low Bouguer anomaly (Büchel, 1992), possibly contributes to the locally elevated topography.

Reflectors A2, B1, B2, and B3 (e.g. Fig. 4) correspond with the thin-skinned nappe reflector proposed by Meissner et al. (1981). Related thrust faults and zones of deformation can contain a fault gauge, which may comprise a few percent of fluids. This results in a decrease in seismic velocities and consequently a negative impedance contrast (negative polarity phases). In our case, the polarities at reflectors A1, A2, B1, B2, and B3 do not fully confirm the proposal of a uniform low-velocity reflector by Meissner (1991), because we observe positive as well as negative polarities along the approximately 30 km extent of these reflectors. At reflectors A1 and A2 polarities could not be recovered, while reflector B1 exhibits negative polarities. However, reflectors B2 and B3 are characterized by varying polarities along their approximately 10 km lateral extent. This observation suggests the presence of nearby patches with typical fault gauge material and/or fluids. This is consistent with the finding that the strength of the reflection signal from B2 is the highest observed one throughout the profile, indicating a strong elastic impedance contrast. Underneath the surface trace of the Eupen Backthrust (Fig. 6) also an exceptionally high reflection strength is found indicating the presence of a fluid-bearing fault gouge, where, compared to the surrounding rock, the fluid proportion is increased, while the density is decreased. This finding is consistent with the interpretation by Meissner (1991). In contrast to that study, we can constrain the negative polarity reflections to the reflectors B2 and B3 with a lateral extent of up to c. 10 km. Additionally, Meissner (1991) proposed that this reflector must be quite thin (40–100 m). Our findings indicate that the negative-polarity reflectors B2 and B3 have even a thickness of approximately 500 m and 600 m, respectively.

Previous tectonic balancing studies on the Eifel Fold and Thrust Belt (e.g., Von Winterfeld and Walter, 1993; Wrede et al., 1993; Von Winterfeld, 1994; Oncken et al., 1999) have integrated surface-to-subsurface projections of structural and stratigraphic outcrop data into cross-section construction, partly compensating the limited signal-to-noise ratio and resolution of the original BELCORP-DEKORP data and nearby seismic-reflection data from industry (BEB8001, BEB8501; see Durst, 1985; Betz et al., 1988). The reprocessing improvement presented in this study allows the mapping of reflection dips at depth with comparatively high confidence; clearly imaging a detachment reflector thus supporting for example the analysis of the relationship between the variable detachment dip and reflection geometries above (Fig. 4). The subsurface interpretation presented shows a concentration of reflectors assigned as thrust faults above the steepest (11°) central detachment segment in the northernmost 50 km of reprocessed BELCORP-DEKORP line 1A (Figs. 4, 6).

Improved structural subsurface imaging of reprocessed BELCORP-DEKORP line 1A furthermore supports wedge-scale geometric balancing (e.g. after Yang et al., 2022; Fig. 7), which is largely independent of dip-azimuth measurements from outcrops or boreholes. Of course, there are several unknowns or uncertainties which we estimate to 10 % for the method and more severely with 20 % - 30 % for the data (e.g., original foreland sloping topography). The estimated shortening of the Eifel Fold and Thrust Belt by around 22 km (equal to c. 22 %; balanced section of Fig. 7a,c. 100 km long) is less than previously balanced in thin-skinned retro-deformation approaches (Von Winterfeld and Walter, 1993; Wrede et al., 1993; Von Winterfeld, 1994; Oncken et al., 1999). Yet the internal reflection structure of the wedge supports the general thin-skinned interpretation of the Eifel Fold and Thrust Belt, adding important detail such as documenting a shallower detachment depth in comparison to these previous studies. Compared to the study by Le Gall (1992), our balancing result provides very similar geometric parameters for the detachment while providing an overall shortening that is half of their results. Based on the high-resolution subsurface imaging of the system of imbricated thrusts and the related backthrusts we identified, we propose a new geological cross section along line 1A.

Table 1
Classification of the reflector types.

Seismic subsection	Tectonic	Stratigraphic	Magmatic
1 (Fig. 5a)	A1, A2, A3, A10, A14, A15, B1, B2, B4, B7, B8	A4, A5, A12, A13	–
2 (Fig. 5b)	C1, C2, C6 – C30, D3, D5, D10	–	–
3 (Fig. 5c)	D4, D5, D16, D17, D20 – D24, D36	D18, D19, D41	–
4 (Fig. 5d)	E7 – E14, E20?	E3 – E6, E16, E17	E1, E2, E23–E39

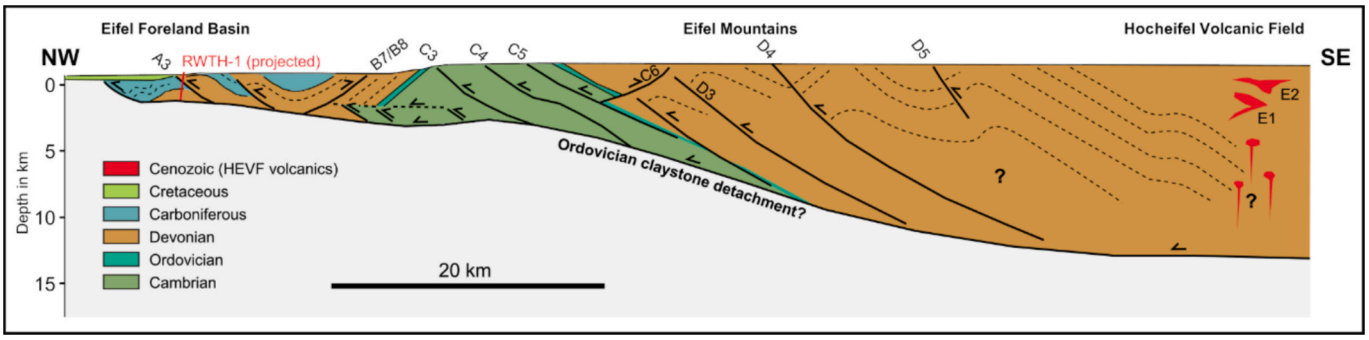

Fig. 8. Schematic geological cross section along BELCORP-DEKORP line 1A integrating the subsurface-reflection interpretation from this study (Figs. 4, 6) with outcrop stratigraphy, surface dip (Nordrhein-Westfalen Geologisches Landesamt, 1992) and projected borehole information of well RWTH-1 (Trautwein-Bruns et al., 2010; Trautwein-Bruns et al., 2011). 2D fault restoration and unfolding above an Ordovician claystone detachment will remain below the 22 km shortening predicted by wedge-scale balancing (Fig. 7).

Fig. 8 is a schematic geological cross section along BELCORP-DEKORP line 1A integrating the subsurface-reflection interpretation from this study (Figs. 4, 6) with outcrop stratigraphy, surface dip (Nordrhein-Westfalen Geologisches Landesamt, 1992) and projected borehole information of well RWTH-1 (Trautwein-Bruns et al., 2010; Trautwein-Bruns et al., 2011). Section construction was such that fault restoration and unfolding above an inferred detachment (Ordovician claystones) remains below the 22 km shortening calculated by wedge-scale balancing (Fig. 7). The section shown is extremely simplified, and the addition of any further stratigraphic detail, in particular the further subdivision of the Devonian into epochs and stages (at the surface and in the subsurface), would make section balancing challenging.

Table 2 presents a comparison of the key regional geometries of the Eifel Fold and Thrust Belt with other terrestrial fold-thrust systems in Europe and overseas, as imaged on deep-reaching seismic reflection data. The observed parameters such as detachment dip, wedge length, thickness, and detachment geometry are comparable with the northern thrust front of the Eastern Alps (Lüschen et al., 2006) and the Variscan fold and thrust front of northern France (Bois, 1991). The Appalachian system of the eastern United States (Pfiffner, 2017) and the Gunnedah basin system of Australia (Pfiffner, 2017) include wedges of over 150 km length and > 20 km thickness, which are much larger and thus probably difficult for potential analogue studies. In contrast, only for few modern mountain belts such as the Alps or Apennines of Europe, the present-day topography can be used for balancing. Nevertheless, existing seismic-reflection data, even if relatively recent, frequently fail to image the roots of fold-thrust systems due to insufficiently long recording times or an inadequate source energy level. Consequently, techniques such as the area-depth-strain method (e.g., Groshong Jr et al., 2012; Schlische et al., 2014; Carboni et al., 2019), the thickness-relief method (Hubert-Ferrari et al., 2005; Gonzalez-Mieres and Suppe, 2011) or the fault-trajectory method are all necessary for geological depth prediction of orogenic detachments (e.g., Eichelberger et al., 2017). In turn, the BELCORP-DEKORP line 1A reprocessing exercise presented here can be regarded as a template study for initiating the reprocessing of a wealth of vintage deep-penetration seismic-reflection data across many mountain belts worldwide, both ancient and modern. The reprocessing of such data clearly has the potential to reveal many previously overlooked geo-scientific subsurface details, which in turn can be used to improve the quality of geological models of fold-thrust systems.

7. Conclusions

The reprocessing of the BELCORP-DEKORP line 1A with state-of-the-art methods such as Fresnel Volume Migration with a newly determined background seismic velocity model reveals new structural details in the lithosphere. This encouraging result shows that more projects reprocessing other datasets, which are easily found in data archives, should be carried out (e.g., DEKORP data centre at GFZ Potsdam). Legacy seismic datasets were previously subject to significant cost in terms of fieldwork and human resources. Many of the recorded data may not be replicated today, for instance, due to stricter legal regulations aimed at safeguarding inhabitants or natural reserves. The generation of enhanced seismic images remains a valuable pursuit, offering insights into tectonic processes and facilitating the advancement of natural resource studies in the context of the transition to renewable energy sources (e.g., geothermal, rare-earth elements).

The reprocessing result of BELCORP-DEKORP line 1A provides a clear delineation of the basal detachment of the Eifel Fold and Thrust Belt, extending for approximately 80 km in length and reaching a depth of c. 10 km. Additionally, the reprocessing result offers insights into basic reflection properties of the detachment. Apart from the

Table 2
Comparison of different detachment structures.

Region / parameter	Eifel, North Variscan deformation front	Eastern Alps	France	U.S.A. Appalachian mountains	Australia
Dataset	BELCORP-DEKORP	TransAlp	N/A	N/A	N/A
Detachment dip	c. 8°	c. 3° - 10°	c. 8° - 10°	c. 3°	c. 0° - 22°
Length in km	c. 80	c. 55	c. 120	> 150	c. 160
Thickness of thrusted material in km	c. 13	c. 12	c. 18	c. 20	c. 25
Shortening in %	c. 22	c. 50 (Pfiffner, 2017)	c. 40–50 (Le Gall, 1992)	c. 17–35 (Reks and Gray, 1983)	unknown
Spacing between major ramps in km	c. 4–7	c. 5–7	c. 5–10	c. 5–15	c. 10–40
Comment	stepwise detachment	flat detachment, few undulations	stepwise detachment	flat detachment	highest dip in the centre
Magmatism	+	–	–	–	–
Source	this study	Lüschen et al., 2006	Bois, 1991	Pfiffner, 2017	Pfiffner, 2017

detachment, reprocessed BELCORP-DEKORP line 1A shows that the Eifel Fold and Thrust Belt comprises several thrust sheets separated by thrusts and backthrusts. The key structural parameters extracted from the reprocessing result form the basis for a regional geometric thrust-wedge restoration, which yields an approximate 22 km of shortening (equal to 22 %) in length. The high resolution reprocessing result and its accuracy eliminate uncertainties about the structure of the Eifel Fold and Thrust Belt raised in previous studies.

The reflective zones interpreted as thrusts are respectively a few hundred meters thick, patchy and associated with a low impedance contrast. This property association can be explained by the presence of crushed rock in a fault gouge zone and the potential existence of a few percent of fluid within the fault zones. It would be interesting to confirm the presence of such fluids, e.g., through the use of electromagnetic methods or even drilling, as fluids can reduce the normal stress on faults increasing the likelihood of failure. The south of reprocessed BELCORP-DEKORP line 1A finally shows a reflective pattern that can be attributed to magmatic processes potentially imprinting pre-existing tectonic structures. These solidified magmatic intrusions produce reflectors that are shorter than those of the main faults, yet exhibit a stronger impedance contrast.

CRediT authorship contribution statement

Dario Eickhoff: Data Processing, Writing - original draft, Writing - review & editing.

Stefan Back: Geological Interpretation, Writing - original draft, Writing - review & editing.

Klaus Reicherter: Geological Interpretation, Writing - original draft, Writing - review & editing.

Joachim Ritter: Conceptional Ideas, Writing - original draft, Writing - review & editing, Supervision.

Declaration of competing interest

The authors declare that they have no known competing financial interests or personal relationships that could have appeared to influence the work reported in this paper.

Acknowledgements

We thank three anonymous reviewers that provided very valuable and constructive comments on the originally submitted manuscript. We thank Stefan Buske and Felix Hloušek of the Freiberg University of Mining and Technology for providing the Fresnel volume migration software and for their extensive support in the preparation of the near surface velocity model and pre-processing of the DEKORP87-1A dataset. We also thank GFZ Data Services for providing access to the seismic dataset of the DEKORP87–1A line used in this study. Open Access funding enabled and organized by Projekt DEAL.

Appendix A. Supplementary data

Supplementary data to this article can be found online at https://doi.org/10.1016/j.tecto.2025.230702.

Data availability

The DEKORP87–1A data used for seismic reflection imaging in this study are available at GFZ Potsdam, see Stiller et al. (2020).

References

Arndt, M., Bißmann, S., Schauenburg, E., Vanbrabant, Y., 2023. Deliverable T2.1.13 – interpretation of seismic data in NRW. Part 1 – results of the reprocessed seismic line DEK87-1A. In: Open File Report Interreg North-West Europe, DGE-Rollout.

Bader, M., Koley, S., van den Brand, J., Campman, X., Bulten, H.J., Linde, F., Vink, B., 2022. Newtonian-noise characterization at Terziet in Limburg—the Euregio Meuse–Rhine candidate site for Einstein Telescope. Class. Quantum Grav. 39 (2), 025009.

Betz, D., Durst, H., Gundlach, T., 1988. Deep structural seismic reflection investigations across the northeastern Stavelot-Venn Massif. Ann. Soc. Geol. Belg. 111, 217–228. https://popups.uliege.be/0037-9395/index.php?id=712.

Bleistein, N., Gray, S.H., 2001. From the Hagedoorn imaging technique to Kirchhoff migration and inversion. Geophys. Prospect. 49 (6), 629–643.

Bois, C., 1991. Geological significance of seismic reflections in collision belts. Geophys. J. Int. 105 (1), 55–69.

Bois, C., Cazes, M., Damotte, B., Galdeano, A., Hirn, A., Mascle, A., Matte, P., Raoult, J.F., Torreilles, G., 1986. Deep seismic profiling of the crust in northern France: the ECORS project. In: Reflection Seismology: A Global Perspective, 13, pp. 21–29.

Büchel, G., 1992. Das Kelberger Hoch. Tiefenstruktur und Geodynamik einer magnetischen Anomalie in der Eifel. Die Geowissenschaften 10 (5), 132–142.

Buske, S., Gutjahr, S., Sick, C., 2009. Fresnel volume migration of single-component seismic data. Geophysics 74 (6), WCA47–WCA55.

Carboni, F., Back, S., Barchi, M.R., 2019. Application of the ADS method to predict a "hidden" basal detachment: NW Borneo fold-and-thrust belt. J. Struct. Geol. 118, 210–223.

Dahm, T., Stiller, M., Mechie, J., Heimann, S., Hensch, M., Woith, H., Schmidt, B., Gabriel, G., Weber, M., 2020. Seismological and geophysical signatures of the deep crustal magma systems of the Cenozoic volcanic fields beneath the Eifel, Germany. Geochem. Geophys. Geosyst. 21, e2020GC009062. https://doi.org/10.1029/2020GC009062.

DEKORP Research Group, Anderle, H.-J., Bittner, R., Bortfeld, R., Bouckaert, J., Büchel, G., Dohr, G., Dürbaum, H.-J., Durst, H., Fielitz, W., Flüh, E., Gundlach, T., Hance, L., Henk, A., Jordan, F., Kläschen, D., Klöckner, M., Meissner, R., Meyer, W., Oncken, O., Reichert, C., Ribbert, K.-H., Sadowiak, P., Schmincke, H.-U., Schmoll, J., Walter, R., Weber, K., Weihrauch, U., Wever, Th., 1991. Results of the DEKORP 1 (BELCORP-DEKORP) deep seismic reflection studies in the western part of the Rhenish Massif. Geophys. J. Int. 106, 203–227. https://doi.org/10.1111/j.1365-246X.1991.tb04612.x.

Demoulin, A., Hallot, E., 2009. Shape and amount of the Quaternary uplift of the western Rhenish shield and the Ardennes (western Europe). Tectonophysics 474, 696–708.

Durst, H., 1985. Interpretation of a reflection-seismic profile across the northeastern Stavelot-Venn Massif and its northern foreland. Neues Jb. Geol. Paläontol. Abh. 171, 441–446. https://doi.org/10.1127/njgpa/171/1985/441.

Eichelberger, N.W., Nunns, A.G., Groshong, R.H., Hughes, A.N., 2017. Direct estimation of fault trajectory from structural relief. AAPG Bull. 101 (5), 635–653.

Eickhoff, D., Ritter, J.R.R., Hloušek, F., Buske, S., 2024. Seismic reflection imaging of fluid-filled sills in the west eifel volcanic field, Germany. Geophys. Res. Lett. 51, e2024GL111425. https://doi.org/10.1029/2024GL111425.

Fekiacova, Z., Mertz, D.F., Renne, P.R., 2007. Geodynamic setting of the Cenozoic Hocheifel volcanism (Germany), part I: $^{40}Ar/^{39}Ar$ geochronology. In: Ritter, J.R.R., Christensen, U.R. (Eds.), Mantle Plumes - A Multidisciplinary Approach. Springer Verlag, Heidelberg, pp. 185–206. https://doi.org/10.1007/978-3-540-68046-8_6.

Fielitz, W., 1992. Variscan transpressive inversion in the northwestern central Rhenohercynian belt of western Germany. J. Struct. Geol. 14 (5), 547–563.

Garcia-Castellanos, D., Cloetingh, S., van Balen, R., 2000. Modelling the Middle Pleistocene uplift in the Ardennes–Rhenish Massif: thermo-mechanical weakening under the Eifel? Glob. Planet. Chang. 27 (1–4), 39–52.

Gonzalez-Mieres, R., Suppe, J., 2011. Shortening Histories in Active Detachment Folds Based on Area-of-Relief Methods.

Groshong Jr., R.H., Withjack, M.O., Schlische, R.W., Hidayah, T.N., 2012. Bed length does not remain constant during deformation: recognition and why it matters. J. Struct. Geol. 41, 86–97.

Hance, L., Dejonghe, L., Ghysel, P., Laloux, M., Mansy, J.L., 1999. Influence of heterogeneous lithostructural layering on orogenic deformation in the Variscan Front Zone (eastern Belgium). Tectonophysics 309 (1–4), 161–177.

Henk, A., 1993. Late orogenic basin evolution in the Variscan internides: the Saar-Nahe Basin, Southwest Germany. Tectonophysics 223 (3–4), 273–290. https://doi.org/10.1016/0040-1951(93)90141-6.

Hollmann, G., Von Winterfeld, C., 1999. Laterale Strukturvariationen eines Vorlandüberschiebungsgürtels. Z. Dtsch. Geol. Ges. 431–450.

Hubert-Ferrari, A., Suppe, J., Van Der Woerd, J., Wang, X., Lu, H., 2005. Irregular earthquake cycle along the southern Tianshan front, Aksu area, China. J. Geophys. Res. Solid Earth 110 (B6).

Kreemer, C., Blewitt, G., Davis, P.M., 2020. Geodetic evidence for a buoyant mantle plume beneath the Eifel volcanic area, NW Europe. Geophys. J. Int. 222 (2), 1316–1332.

Le Gall, B., 1992. The deep structure of the Ardennes Variscan thrust belt from structural and ECORS seismic data. J. Struct. Geol. 14 (5), 531–546.

Lüschen, E., Borrini, D., Gebrande, H., Lammerer, B., Millahn, K., Neubauer, F., Nicolich, R., TRANSALP Working Group, 2006. TRANSALP—deep crustal Vibroseis and explosive seismic profiling in the Eastern Alps. Tectonophysics 414 (1–4), 9–38.

Mechie, J., Prodehl, C., Fuchs, K., 1983. The long-range seismic refraction experiment in the Rhenish Massif. In: Fuchs, K., von Gehlen, K., Mälzer, H., Murawski, H., Semmel, A. (Eds.), Plateau Uplift. Springer, Berlin, Heidelberg, pp. 260–275. https://doi.org/10.1007/978-3-642-69219-2_31.

Meissner, R., 1991. The Dekorp surveys: major results in tectonic and reflective styles. In: Meissner, R., Brown, L., Dürbaum, H.-J., Franke, W., Fuchs, K., Seifert, F. (Eds.), Continental Lithosphere: Deep Seismic Reflections, AGU Geodynamic Series, vol. 22, pp. 69–76. https://doi.org/10.1029/GD022p0069.

Meissner, R., Bortfeld, R. (Eds.), 1990. DEKORP Atlas - Results of Deutsches Kontinentales Reflexionsseismisches Programm. Springer, Heidelberg. https://doi.org/10.1007/978-3-642-75662-7.

Meissner, R., Bartelsen, H., Murawski, H., 1981. Thin-skinned tectonics in the northern Rhenish Massif, Germany. Nature 290, 399–401. https://doi.org/10.1038/290399a0.

Meyer, W., Stets, J., 2007. Quaternary uplift in the Eifel area. In: Mantle Plumes: A Multidisciplinary Approach. Springer Berlin Heidelberg, Berlin, Heidelberg, pp. 369–378.

Nordrhein-Westfalen Geologisches Landesamt, 1992. Geologische Karte von Nordrhein-Westfalen <1:100000> / Geolog. Landesamt Nordrhein-Westfalen C 5502, Aachen, Erläuterungen. Krefeld: N.p., 1992. Print.

Oncken, O., Von Winterfeld, C., Dittmar, U., 1999. Accretion of a rifted passive margin: the late Paleozoic Rhenohercynian fold and thrust belt (middle European Variscides). Tectonics 18 (1), 75–91.

Pfiffner, O.A., 2017. Thick-skinned and thin-skinned tectonics: a global perspective. Geosciences 7 (3), 71.

Reicherter, K., Froitzheim, N., Jarosinski, M., Badura, J., Franzke, H.-J., Hansen, M., Hübscher, C., Müller, R., Poprawa, P., Reinecker, J., Stackebrandt, W., Voigt, T., von Eynatten, H., Zuchiewicz, W., 2008. Chapter 19. Alpine tectonics north of the Alps. In: McCann, T. (Ed.), The Geology of Central Europe, 2. Geol. Soc, London, pp. 1233–1286. Mesozoic and Cenozoic. ISBN 978-1-86239-265-6.

Reinig, F., Wacker, L., Jöris, O., Oppenheimer, C., Guidobaldi, G., Nievergelt, D., Adolphi, F., Cherubini, P., Engels, S., Esper, J., Land, A., Lane, C., Pfanz, H., Remmele, S., Sigl, M., Sookdeo, A., Büntgen, U., 2021. Precise date for the Laacher See eruption synchronizes the Younger Dryas. Nature 595 (7865), 66–69.

Reks, I.J., Gray, D.R., 1983. Strain patterns and shortening in a folded thrust sheet: an example from the southern Appalachians. Tectonophysics 93 (1–2), 99–128.

Ribbert, K.-H., Geologischer Dienst Nordrhein-Westfalen, & Geologischer Dienst Nordrhein-Westfalen, 2010. Geologie im Rheinischen Schiefergebirge. Geologischer Dienst NRW.

Ritter, J.R., Jordan, M., Christensen, U.R., Achauer, U., 2001. A mantle plume below the Eifel volcanic fields, Germany. Earth Planet. Sci. Lett. 186 (1), 7–14.

Schlische, R.W., Groshong Jr., R.H., Withjack, M.O., Hidayah, T.N., 2014. Quantifying the geometry, displacements, and subresolution deformation in thrust-ramp anticlines with growth and erosion: from models to seismic-reflection profile. J. Struct. Geol. 69, 304–319.

Schmincke, H.U., 2007. The Quaternary Volcanic fields of the East and West Eifel (Germany). In: Ritter, J.R.R., Christensen, U.R. (Eds.), Mantle Plumes. Springer, Berlin, Heidelberg, pp. 241–322. https://doi.org/10.1007/978-3-540-68046-8_8.

Silverii, F., Mantiloni, L., Rivalta, E., Dahm, T., 2023. Lithospheric sill intrusions and present-day ground deformation at Rhenish Massif, Central Europe. Geophys. Res. Lett. 50, e2023GL105824. https://doi.org/10.1029/2023GL105824.

Stiller, M., Kaerger, L., Agafonova, T., Krawczyk, C., Oncken, O., Weber, M., Former DEKORP Project Leaders, Former DEKORP/BELCORP Research Group, Former DEKORP Processing Centre, 2020. Deep Seismic Reflection Profile DEKORP 1987-1A Across the Western Rhenish Massif, West Germany/East Belgium. GFZ Data Services. https://doi.org/10.5880/GFZ.DEKORP-1A.001.

Trautwein-Bruns, U., Schulze, K.C., Becker, S., Kukla, P.A., Urai, J.L., 2010. In situ stress variations at the Variscan deformation front — results from the deep Aachen geothermal well. Tectonophysics 493, 196–211. https://doi.org/10.1016/j.tecto.2010.08.003.

Trautwein-Bruns, U., Hilgers, C., Becker, S., Urai, J.L., Kukla, P.A., 2011. Fracture and fault systems characterising the intersection between the lower Rhine Embayment and the Ardennes-Rhenish Massif - results from the RWTH-1 well, Aachen, Germany. Z. Dtsch. Ges. Geowiss. 162, 251–275. https://doi.org/10.1127/1860?1804/2011/0162.

Voges, A., Toloczyki, M., Zitzmann, A., Wittekindt, H., Trurnit, P., 2006. Geological Map of Germany 1:1,000,000 (GK1000). https://gdk.gdi-de.org/geonetwork/srv/api/records/1C60DDA9-EF73-47B9-9ED7-FCD22B3226C1.

Von Winterfeld, C.H., 1994. Variszische Deckentektonik und devonische Beckengeometrie der Nordeifel – Ein quantitatives Modell, Dissertation, Aachener Geowissenschaftliche Beiträge. RWTH Aachen.

Von Winterfeld, C., Walter, R., 1993. Die variszische Deformationsfront des nordwestlichen Rheinischen Schiefergebirges. Ein bilanziertes geologisches Tiefenprofil über die Nordeifel. In: Neues Jahrbuch für Geologie und Paläontologie. Monatshefte, 1993, 5, pp. 305–320.

Wrede, V., 2000. Zur Bedeutung der Aachener Steinkohlenlagerstätte für das Verständnis der Variscischen Orogenfront in Mitteleuropa. Zbl. Geol. Paläont. Teil I 1999 (3–4), 199–215.

Wrede, V., Drozdzewski, G., Dvorak, J., 1993. On the structure of the Variscan front in the Eifel-Ardennes-area. In: Gayer, R.A., Greiling, O., Vogel, K. (Eds.), Rhenohercynian and Subvariscan Fold Belts. Vieweg, Braunschweig/Wiesbaden, pp. 269–296.

White, R.S., Smith, L.K., Roberts, A.W., Christie, P.A.F., Kusznir, N.J., & rest of the iSIMM Team The iSIMM team includes, in addition to the other authors Roberts, A.M., Healy, D., Spitzer, R., Chappell, A., Eccles, J.D., Fletcher, R.,Hurst, N., Lunnon, Z., Parkin, C.J., Tymms, V.J., 2008. Lower-crustal intrusion on the North Atlantic continental margin. Nature, 452(7186), 460-464.

Yang, X., Sanderson, D.J., McNeill, L.C., Peel, F.J., 2022. The effects of initial wedge taper on area-balancing restoration of a fold-thrust belt. AAPG Bull. 106 (1), 21–41.